Molecular and Cellular Biochemistry
https://doi.org/10.1007/s11010-020-03693-y

Nucleation and kinetics of SOD1 aggregation in human cells for ALS1

Aron Workman[1,2]

Received: 11 March 2019 / Accepted: 29 January 2020

Abstract
Aberrant structural formations of Cu/Zn superoxide dismutase enzyme (SOD1) are the probable mechanism by which circumscribed mutations in the *SOD1* gene cause familial amyotrophic lateral sclerosis (ALS1). SOD1 forms aberrant structures which can proceed by nucleation to insoluble aggregates. Here, the SOD1 aggregation reaction was investigated predominantly by time-course studies on ALS1 variants G85R, G37R, D101G, and D101N in human embryonic kidney cells (HEK293FT), with analysis by detergent ultracentrifugation extractions and high-resolution PAGE methodologies. Nucleation was found to be pseudo-zeroth order and dependent on time and concentration at constant 37.0 °C and pH 7.4. The predominant subsets of the total SOD1 expression set which comprised the nucleation phase were both soluble and insoluble inactive monomers, trimers, and hexamers with reduced intra-disulfide bonds. Superoxide exposure via paraquat initiated the formation of SOD1 trimers in untransfected SH-SY5Y cells and increased the aggregation propensity of G85R in HEK293FT. These data show the kinetic formation of aberrant SOD1 subsets implicated in ALS1 and indicate that superoxide substrate may initiate its radical polymerization. In an instance of the utility of methodological reductionism in molecular theory: though many ALS1 variants retain their global enzymatic activity, the SOD1 subsets most implicated in causing ALS1 do not retain their specific activity.

Keywords Superoxide dismutase 1 (SOD1) · Polyacrylamide gel electrophoresis (PAGE) · High-resolution colorless native PAGE (hrcN-PAGE) · Familial amyotrophic lateral sclerosis (ALS)

Introduction

The *SOD1* gene encodes Cu/Zn superoxide dismutase (SOD1), which is a complex enzyme that is widely expressed in the cytosol of aerobic cells [1]. The primary function of SOD1 is to convert superoxide radicals to energy and waste at a rate of over one billion radicals per second, with net reaction: $2O_2^- + 2H^+ \rightarrow O_2 + H_2O_2$ (EC 1.15.1.1) [2–4]. SOD1 probably extinguishes superoxide by a direct deionization to dioxygen [5, 6], which is an energetically favorable charge transfer reaction with an uncatalyzed rate of femtoseconds [7]. Two billion years of aerobic evolution equipped SOD1 with specialized metallic and sulfidic molecular components. The active enzyme binds a copper ion (Cu), a zinc ion (Zn), an oxidized intra-disulfide, and an active site salt bridge, per subunit, among other co-factors [8]. Nascent SOD1 translate is biosynthesized as an un-metallated, intra-reduced, monomeric, destabilized, and inactive polypeptide product that is processed to a fully metallated, intra-oxidized, dimeric, stable, and active enzyme, with net reaction: $2\varnothing/\varnothing\text{-Rd-SOD1} + 2Cu^{2+} + 2Zn^{2+} \rightarrow (Cu/Zn–Ox–SOD1)_2$. This maturation reaction is catalyzed on the order of the picosecond by dioxygen and an exclusive copper chaperone paralog (CCS) [9–14]. SOD1 maturation is prerequisite to its catalysis [15–17]: Cu, Zn, and an oxidized intra-disulfide are all required bindings for its reaction mechanisms [18, 19].

Amyotrophic lateral sclerosis (ALS) is a neurodegenerative disease without effective treatment that causes the rapid onset of paralysis [20]. Its prevalence is commonly reported at 30,000 global patients. The majority of ALS cases are currently diagnosed "sporadic", but a growing compendium of confirmed genetic loci bolster the notion that ALS is of predominantly genetic origin [21, 22]. Among causal familial ALS genes, hundreds of predominantly

✉ Aron Workman
aworkman@ufl.edu; aron@axoxy.com

[1] Present Address: AXOXY Laboratories, Weston, Florida 33326, USA

[2] McKnight Brain Institute, University of Florida, Gainesville, Florida 32610, USA

Published online: 13 February 2020

missense substitution mutations encoded within *SOD1* (21q22.11) claim more global familial ALS patients than *FUS*, *UBQLN2*, and *TARDBP* combined [23, 24]. Certain circumscribed SOD1 variants initiate and sustain ALS1 dose-dependently [25, 26]. Additionally, these variants are not pathogenic due to a global loss of activity [27], and SOD replacement therapy is not effective; thus ALS1 is frequently described as a "gain-of-function" disease. Here I studied the SOD1 aspartate 101 variants D101G and D101N, and the SOD1 glycine → arginine variants G85R and G37R. D101G and D101N were studied for their similar clinical metrics [23], yet reportedly only minor biochemical similarities [28], which is irregular and hitherto a paradox [29, 30]. G85R and G37R were studied because they are prevalent variants with similar electrostatic identities which can be useful discriminators due to their irregular PAGE migration [27, 31]. I also conducted studies on the prevalent variants G93A, A4V (the most common ALS1 subpopulation in North America), and experimental compound copper ablation variant H46R/H48Q [32, 33].

SOD1 associated with ALS1 forms fibrillar polymers with structures described as "nanotubes" [34], and "pore-like" [35]. The SOD1 expression pool can accumulate monomeric [36, 37], metal-free [38], and intra-reduced subsets [39], which are particularly prone to the nucleation of lower-order polymers and then higher-order aggregates. Lower-order polymerization was found non-stochastically reproducible in HEK293FT [40]. Deleterious formations of SOD1 in the symptomatic spinal cord manifest as detergent-insoluble high molecular weight aggregates. Every of dozens of ALS1 variants thus far assayed form significant detergent-insoluble species that are either antecedent or concomitant with the progression of ALS1 [25, 28, 29, 41–48], whereas WT and other innocuous variants remain persistently soluble [49, 50]. The formation of insoluble aggregates predicts deleterious SOD1, whereas the absence of insoluble aggregates predicts innocuous SOD1. A common dichotomy drawn on ALS1 theories of disease is oxidation versus aggregation, with few reports on the possibility of both [51]. Delineating the nucleation formation may be crucial to a therapeutic approach to ALS1 because that is the threshold event wherein SOD1 begins to form toxic polymers (ranging from trimers to mass aggregates). SOD1 also forms fragmentation products when stressed with high concentrations of superoxide [52]. Paraquat (methyl viologen) is a physiological superoxide radical generator within the cytosol [53]. The SOD1 trimer was first shown induced to formation through the use of paraquat [54], though it was not then identified as such.

The reaction mechanisms and kinetics of SOD1 aggregation have been previously explored using a variety of unique model systems [40, 55, 56], but none have yet reported on the kinetics and molecular states of SOD1 subsets within the biochemical context of human cells, which may be an essential distinction for the SOD1 aggregation reaction specifically [57, 58]. The experiments of this study employed HEK293FT coupled with a robust detergent ultracentrifugation extraction—the detergent ultracentrifugation extraction to detect and quantify SOD1 aggregation is more consistent and has a superior limit of detection than that of analytical size exclusion chromatography. Detergent ultracentrifugation for the quantitative detection of soluble and insoluble SOD1 subsets is a well-established model system [29, 41, 44, 59, 60], and the relative aggregation propensity metric is robust with high inter-laboratory precision [25, 28, 43].

Investigating the nucleation and kinetics of SOD1 aggregation is critical to ALS1 research. The purpose of this study was to elucidate the non-native SOD1 formations which comprise the aggregation reaction for eventual diagnostic and therapeutic intent. If identified, the aggregation nucleus could become a key drug discovery and development target.

Methods

Plasmids and molecular cloning

Plasmid cDNA constructs encoding the human *SOD1* GOIs were obtained by PCR point mutagenesis of the WT template that was encoded within the mammalian expression vector pEF-BOS [61]. pEF-BOS was customized with the 5′ addition of NcoI and the 3′ addition of SalI for subcloning [28]. WT, A4V, G37R, G85R, G93A, H46R/H48Q, D101G, and D101N were previously cloned as described [27, 62], and fresh clones were prepared for this work. Milligram quantities of ~ g/L cDNA were prepared by double cesium chloride/ethidium bromide centrifugation density gradients. The identities of the cDNA constructs were twice verified by automated sequencing at the University of Florida DNA Sequencing Core (Gainesville, Florida).

Cell culture transfections and harvests

The source for the HEK293FT (human embryonic kidney) cells was Fisher Scientific #R70007 (RRID:CVCL_6911). The source for the NIH3T3 cells was ATCC #CRL-1658 (RRID:CVCL_0594). The source for the N2a (mouse neuroblastoma) cells was ATCC #CCL-131 (RRID:CVCL_0470). The source for the SH-SY5Y (human neuroblastoma) cells was ATCC #CRL-2266 (RRID:CVCL_0019). The N2a and SH-SY5Y cells were treated with 12 μM retinoic acid to induce neuronal differentiation. Cells were grown at constant 37.0 °C with 5.0% CO_2 in lysine-coated dishes containing DMEM with 10% FBS (supplemented with L-glutamine). Micrographs were recorded at regular intervals with a standard optical microscope. Cells that were refreshed from

cryostat were maintained at one-third to four-fifths confluency before passaging. To transfect the cells, the media of the confluent 60 mm dishes were replaced with Opti-MEM, and the cells were treated with Lipofectamine 2000 (Thermo Scientific) and 4.00 µg cDNA construct. Media were added to the dishes 4 h later. Manual harvests began 6 h after transfection, and at 6 h intervals thereafter, accurate to within 6 min. At harvest time, the media were aspirated, the dishes were rinsed with PBS, cells were scraped with cell lifters into microcentrifuge tubes and placed on ice, rinsed twice with iced PBS, and then flash frozen. Cell pellets were stored at − 80 °C for a maximum of 4 months.

Paraquat exposures

Concentrated paraquat solutions were prepared from a crystalline powder with high caution as a human health hazard; replicates of hazardous experiments were reduced to a minimum of two. The paraquat solutions were pre-mixed with standard media before dish media replacements that were incubated for 16 h.

Detergent ultracentrifugation extractions

The detergent ultracentrifugation extraction method was previously well described [28, 29, 59, 60]. Intact cell pellets were thawed on ice and resuspended in 100 µL 1xTEN (10 mM Tris pH 7.4, 1 mM EDTA pH 8.0, 100 mM NaCl). 100µL 1xTEN with 1% Nonidet P40 (NP-40) and 1% protease inhibitor cocktail (PI, Roche) were added for a final concentration of 0.5% NP-40. This mixture was then sonicated and centrifuged for 5 min at > 100,000x*g* in a Beckman airfuge. The soluble portion was saved as "S1" and the pellet was resuspended in 200 µL of 1 × TEN with 0.5% NP-40 and 1% PI. The pellet was then sonicated and centrifuged again, this time discarding the soluble fraction. The pellet was resuspended and sonicated in 1xTEN with 0.5% NP-40, 0.25% SDS, 0.5% deoxycholate, and 1% PI, and the insoluble portion was saved as "P2". S1 and P2 fractions were consistently assayed at just one freeze/thaw cycle total.

Experimental PAGE conditions

For the freeze/thaw extract (F/T), a cell pellet was resuspended in TN + 0.1% NP-40 with PI and then dunked in a dry ice/ethanol slurry, followed by a brief sonication and centrifugation at 500 *g* for 5 min for clarity. Experiments for the delineation of the intra-disulfide bond were also treated with iodoacetamide in the sample buffer. For high-resolution colorless native PAGE (hrcN-PAGE), equivalent samples from S1, P2, or F/T extracts were loaded with ~ 20% glycerol on 1xTG gels without SDS, and run at 100 constant volts (cV) for 8 h at 4 °C. To resolve activity, low concentration polyacrylamide gels were used (8%); to resolve polymers, high-concentration polyacrylamide gels were used (15% or 4–20%). Certain gels were processed with an in-gel reduction: 2% SDS 2% βME 1xTG and microwaved for pulses of 20 s each for 2 min total.

Nitroblue tetrazolium assays

Total cell lysates were extracted by F/T and processed with hrcN-PAGE in 1xTG buffer with 20% methanol at 100cV for 4 to 6 h at 4.0 °C. The gel was retrieved in 50 mM potassium bicarbonate buffer at pH 7.6 containing 65 µg/mL riboflavin and 280 µg/mL nitro blue tetrazolium, where it was incubated for 2 to 40 min before a buffer swap to 0.1% TEMED. The gel was exposed for imaging with bright white light on an Agfa Duoscan.

Western immunoblotting

BCA assay with BSA standards was used to determine the protein concentrations of samples. 5 µg S1 and 20 µg P2 samples were prepared to 20 µL solution in 1xTEN with Laemmli buffer (5% βME). Samples were boiled at 96 °C for 6 min and loaded onto an 18% gel for PAGE. The gel was then transferred to nitrocellulose membrane for 2 h at 400 mA and incubated for 15 to 40 min in 5% low fat dry milk of PBS with 0.1% Tween-20 (PBS-T). Immunoblots were 1° incubated with a 1:5000 mouse/human SOD1 antibody that binds amino acids 124 to 136 (125 to 137) with high specificity [27], rinsed three times in PBS-T, and then 2° incubated with a 1:2500 goat anti-rabbit HRP antibody for 1.0 h. Immunoblots were rinsed with PBS-T, treated with chemiluminescence reagents, and exposed on a Fujifilm LAS-3000. Immunoblots were quantified with ImageJ 1. The relative aggregation propensity metric was calculated by detecting the signal of P2 relative to the signal of S1 relative to the same for A4V at 24 h [28]. Immunoblot bands were within the linear dynamic range except where a different exposure was intentional for the qualitative identification of minor species.

Net charge calculations

Net charge (and isoelectric point) calculations were automated using the python programming language. The Henderson–Hasselbalch equation was used to calculate the net charge of each sequence as a function of pH by the sum $\sum_{\mathrm{i}}^{\mathrm{n}} \frac{1}{1+10^{\mathrm{pK}-\mathrm{pH}}}$ to yield the weighted base formula $Z = \sum_i N_i \frac{10^{pKa_i}}{10^{pH}+10^{pKa_i}} - \sum_j N_j \frac{10^{pKa_j}}{10^{pH}+10^{pKa_j}}$ [63, 64], where N_{i} and pKa_{i} are the amino acid counts and *pKa* values of the *N*-terminus and basic residues (H, R, K), and N_{j} and pKa_{j} are the amino acid counts and *pKa* values of the *C*-terminus and acidic residues (D, E, C, and Y).

Logistic statistics

Ordinary fit least-squares were used to compute the statistical parameters and best fits, beginning with the integrated logistic equation: $L/\left(1+e^{-k(t-t_0)}\right)$. The initial parametric values were as follows: L=max{relative aggregation propensity}; k=min{relative aggregation propensity}; $t_0=[\tilde{t}]$; the functions easily converged with parametric lower bounds of 0 and upper bounds of ∞. Five sigmoidal functions were utilized to model the time-course data [65]: 1. Logistic function: $m(t)=m_0\cdot\left[1+e^{-k*(t-t_0)}\right]^{-1}$; 2. Base autocatalytic model function: $m_0\cdot\left[\left(\frac{(-k_1)\cdot m_0}{(-k_0)+(-k_1)\cdot m_0}\right)+\left(\frac{-k_0}{(-k_0)+(-k_1)\cdot m_0}\right)\cdot e^{((-k_0)+(-k_1)\cdot m_0)\cdot t}\right]^{-1}$; 3. Gompertz model function: $m_0\cdot\left(1-\Delta\cdot e^{-e^{K}\cdot(t-t_m)}\right)$; 4. Monomer partitioning model function: $m_0\cdot(f\cdot e^{k_0\cdot t}+(1-f)\cdot e^{\left(\frac{-k_1\cdot f\cdot m_0}{-k_0}\right)\cdot(1-(-k_0\cdot t)-e^{k_0\cdot t})}$; 5. Exponential growth function: $m_0\cdot\left(1-\Delta\cdot e^{k_1\cdot t}\right)$. The goodness of the sigmoid functions was programmatically evaluated by a derivative of the Akaike information criterion (AIC) [21]: $AIC=2p+N\left(\ln 2\pi+1-\ln N+\ln\sum_{i=1}^{n}x_i^2\right)$.

Results

Western immunoblots of the soluble and insoluble fractions of SOD1 over time

SOD1 aggregation was studied by time-course experiments where HEK293FT were transfected with a cDNA construct and then harvested every 6 h for a total of 2 days. The soluble and insoluble fractions of WT and each of four ALS1 variants were extracted by detergent ultracentrifugation; the results were graphed on the western immunoblots of Fig. 1.

G85R, G37R, D101G, and D101N exhibited robust aggregation by a two-day harvest time, as given in Fig. 1a-d, whereas WT did not form detectable aggregates even up to an extended harvest time of over one week, as given in Fig. 1e. The soluble fractions of Fig. 1 show that expression began at a harvest time on or before 6 h, and that expression levels stabilized at harvest times of between 12 and 18 h. The aberrant structures that formed thereafter were predominantly comprised of insoluble SOD1 subsets which migrated at the monomeric position, with minor species that migrated at higher-order positions found SDS-resistant.

High-resolution PAGE experiments on critical SOD1 subsets

Detailed information on the molecular composition of the SOD1 subsets was obtained by the high-resolution PAGE experiments of Fig. 2. An extended western immunoblot time-course study of insoluble SOD1 formations in the D101N variant is given in Fig. 2a. Nucleation was further studied by hrcN-PAGE experiments on D101G and D101N at 42 h, given in Fig. 2b–c. The nucleation of soluble G85R trimers and hexamers as a function of the transfected cDNA mass is given in Fig. 2d.

The high-resolution PAGE to western immunoblot experiment on D101N given in Fig. 2a shows an apparent hexamer at 24 h, even prior to the formation of trimers at 30 h. The insoluble apparent hexamer immediately precedes the insoluble aggregation of the monomer, which may be indicative of a complex nucleation-dependent reaction involving trimeric intermediates. The hexamer is possibly a dimer of trimers. Pentamer SOD1 and higher-order multimers ($n\geq 5$) are "apparent": a number of repetitions of high-resolution discriminations such as that available in Figs. 1 and 2a give confidence in the migration positions up to the tetramer

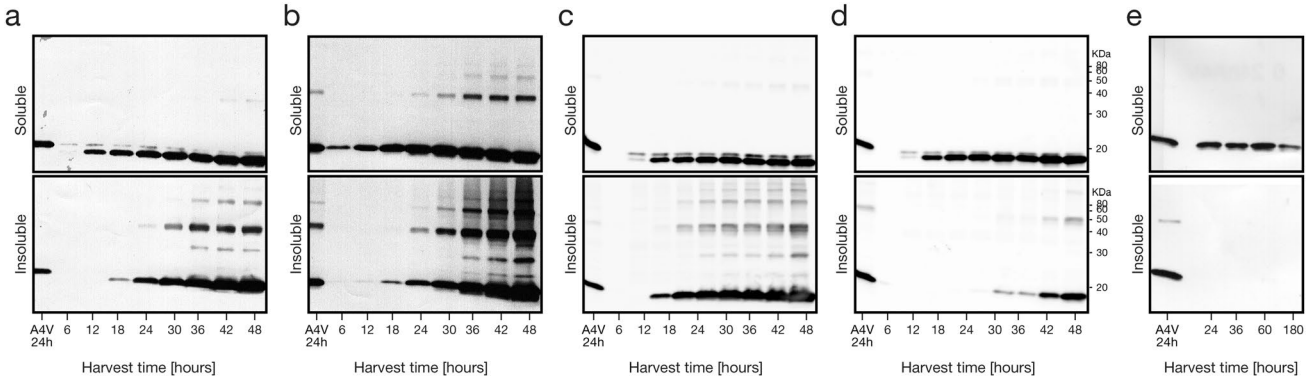

Fig. 1 ALS1 variants G85R, G37R, D101G, and D101N accumulate robust aggregates over time whereas WT remains persistently soluble. Detergent ultracentrifugation extracts of HEK293FT cells that expressed SOD1 variants **a** G85R, **b** G37R, **c** D101G, **d** D101N, or **e** WT; S1 (soluble) and P2 (insoluble) fractions were graphed by western immunoblot versus harvest time; A4V harvested at 24 h (A4V 24 h) was the quantitative standard. **a-d** Extracts of ALS variants **a** G85R, **b** G37R, **c** D101G, or **d** D101N, at 6 h harvest times for up to 2 days (6, 12, 18, 24, 30, 36, 42, and 48 h) ($n\geq 4$). **e** Extracts of WT SOD1 at harvest times of 24, 36, 60, and 180 h ($n=3$)

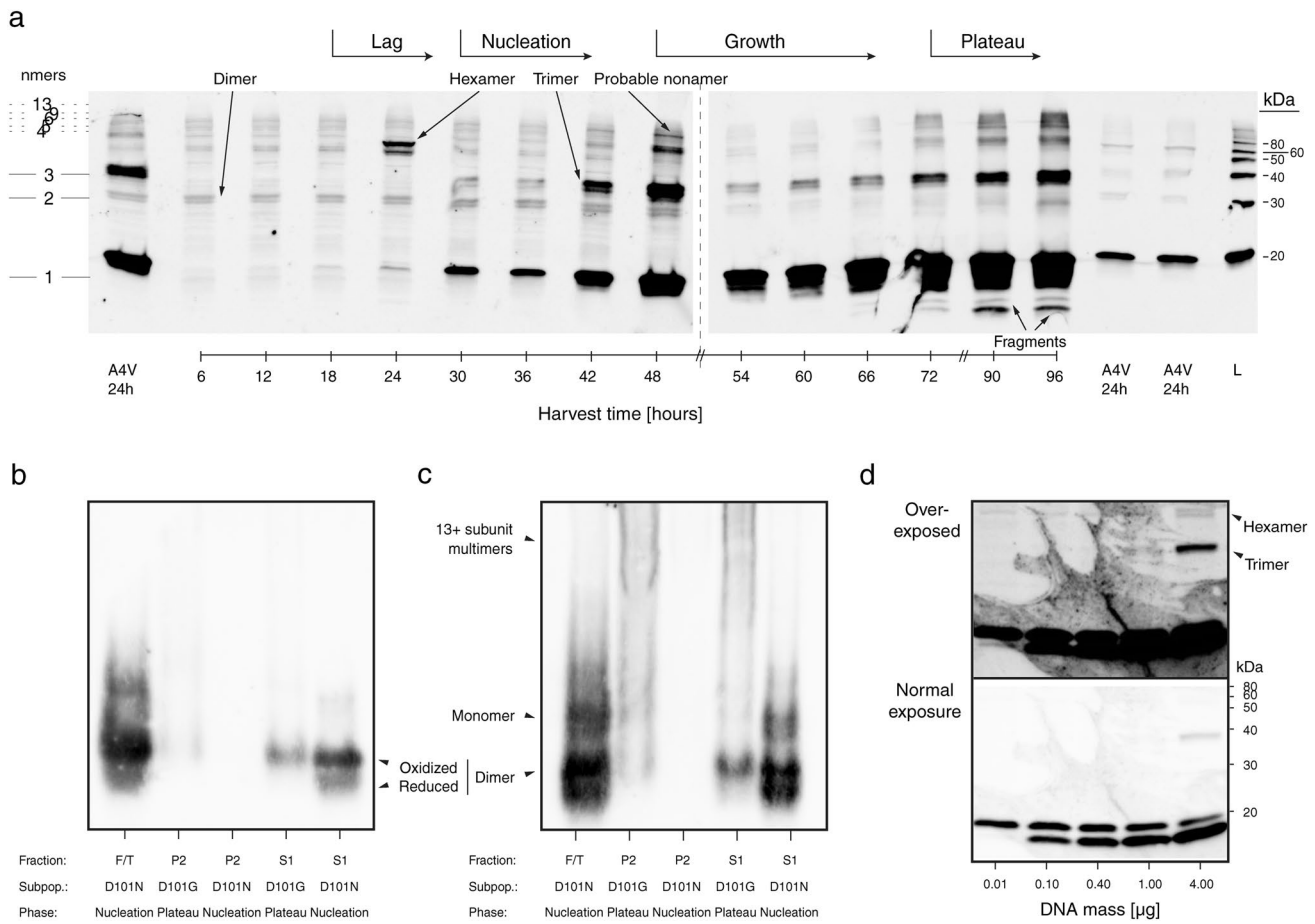

Fig. 2 The nucleation and growth phases of SOD1 aggregation proceed by intra-disulfide-reduced trimeric intermediates that can be induced by superoxide radical. Subsets of non-native formations graphed by high-resolution PAGE versus **a** harvest time or **b-d** experimental condition for SOD1 variants **d** G85R, **a** D101N, and **b**, **c** D101N and D101G. **a** P2 fractions of HEK293FT that expressed D101N at harvest times of up to 4 days (6, 12, 18, 24, 30, 36, 42, 48, 54, 60, 66, 72, 90, and 96 h); A4V harvested at 24 h (A4V 24 h) was the quantitative standard; apparent dimers, trimers, hexamers, and fragments are labeled according to the molecular weight ladder (L); the four logistic phases of SOD1 aggregation are identified (lag, nucleation, growth, and plateau). **b-c** Freeze–thaw (F/T), P2, and S1 fractions of HEK293FT that expressed D101N or D101G at a harvest time of 42 h **b** with βME/SDS in-gel reduction, and **c** without in-gel reduction; the oxidized and reduced dimer, monomers, and 13 + subunit multimers are identified. **d** Representative western immunoblot of G85R controlled to variable cDNA mass collected by freeze–thaw extract at an 18 h harvest time ($n = 3$); the "normal exposure" blot was within the linear dynamic range, but the "over-exposed" blot enabled examination of the trimers and hexamers

($n \leq 4$), but the exact order of the highest order multimers cannot be easily determined within this methodology. Apparent nonamers are observed concomitant within the high molecular weight formations.

Fragments form during the plateau phase beginning at approximately 3 days. The states of the intra-disulfide bonds of the various subsets captured were determined using hrcN-PAGE with discriminations by in-gel reduction, for instance, in Fig. 2b–c. During the aggregation plateau, the intra-disulfide bond was fully reduced; during the aggregation nucleation, the intra-disulfide bond was both oxidized and reduced.

To titrate transfection versus expression, cells were transfected with increasing masses of G85R cDNA at 24 and 48 h for western immunoblotting. Figure 2d shows that SOD1 nucleation is dependent on the expression concentration of SOD1. G85R had the largest nucleation phase fluctuations of the four variants, but that nucleation was still confirmed concentration-dependent; G85R nucleation fluctuations are apparently an innate property of that variant. The cDNA titration of Fig. 2d that exploited the anomalous migration of G85R to delineate the expression subsets from the endogenous WT subsets show that nucleation is concentration dependent. As quality assurance for the cell culture system that was used, these experiments incidentally confirmed a linear dynamic range of the expressed protein mass versus the mass of transfected cDNA.

Quantified aggregation of SOD1 polymers with logistic fits

Data sets of SOD1 aggregation as a function of harvest time at the monomer, dimer, trimer, and hexamer positions were quantified and fit with the linear function and five distinct sigmoidal functions (autocatalytic, exponential, logistic, Gompertz, and monomer partitioning), with the -AICc metric of best fit. Quantified plots of the relative aggregation propensity of each of four familial ALS1 variants as a function of harvest time with its autocatalytic functions are given in Fig. 3. D101G and D101N were reported at extended time-course studies of several days in Fig. 3a. G85R, G37R, D101G, and D101N are given at two-day studies in Fig. 3b–e.

The net aggregation reaction was pseudo-zeroth order (or second order) for G85R, G37R, D101G, and D101N. Excluding the nucleation phase, SOD1 aggregation kinetics were linear with $R^2 > 0.8$. D101G had the fastest linear rate of aggregate formation ($m = 3.51$), whereas experimental compound copper knockout H46R/H48Q had the slowest linear rate of aggregate formation ($m = 0.189$); however, D101G was observed well into its plateau at 5 days whereas H46R/H48Q had just begun its nucleation at 2 days. The logistic function was "not inadequate" for any variant by the replicates test for logistic fit: 0.13 for D101G, 0.065 for D101N, 0.83 for G85R, and 0.71 for G37R. The R^2 for logistic fit values was 0.89 for D101G, 0.96 for D101N, 0.76 for G85R, and 0.95 for G37R. However, the linear function was found deviant according to the Runs test: 0.039* for D101G and 0.028* for D101N. The R^2 for linear fit values was 0.88 for D101G, 0.93 for D101N, 0.98 for G85R, and 0.96 for G37R. The relative aggregation propensities of G93A and H46R/H48Q at the monomeric position were also recorded as a function of harvest time every 6 h for 48 h: G93A had a linear R^2 of 0.90, and H46R/H48Q had a linear R^2 of 0.58; G93A and H46R/H48Q fit best to the autocatalytic model: G93A had a k_0 of 3.5 and k_1 of 1.2, whereas H46R/H48Q had a k_0 of 2.4 and k_1 of 3.4; the relative aggregation propensity of H46R/H48Q approached 0.5 whereas that of G93A approached 3 at a harvest time of 48 h (Fig. 4).

Parallel hrcN-PAGE for the delineation of the soluble subsets of SOD1

The soluble subsets of WT, UT, D101G, D101N, A4V, G93A, and G85R were graphed by hrcN-PAGE under varying methodological conditions, which are given in Fig. 5a–c.

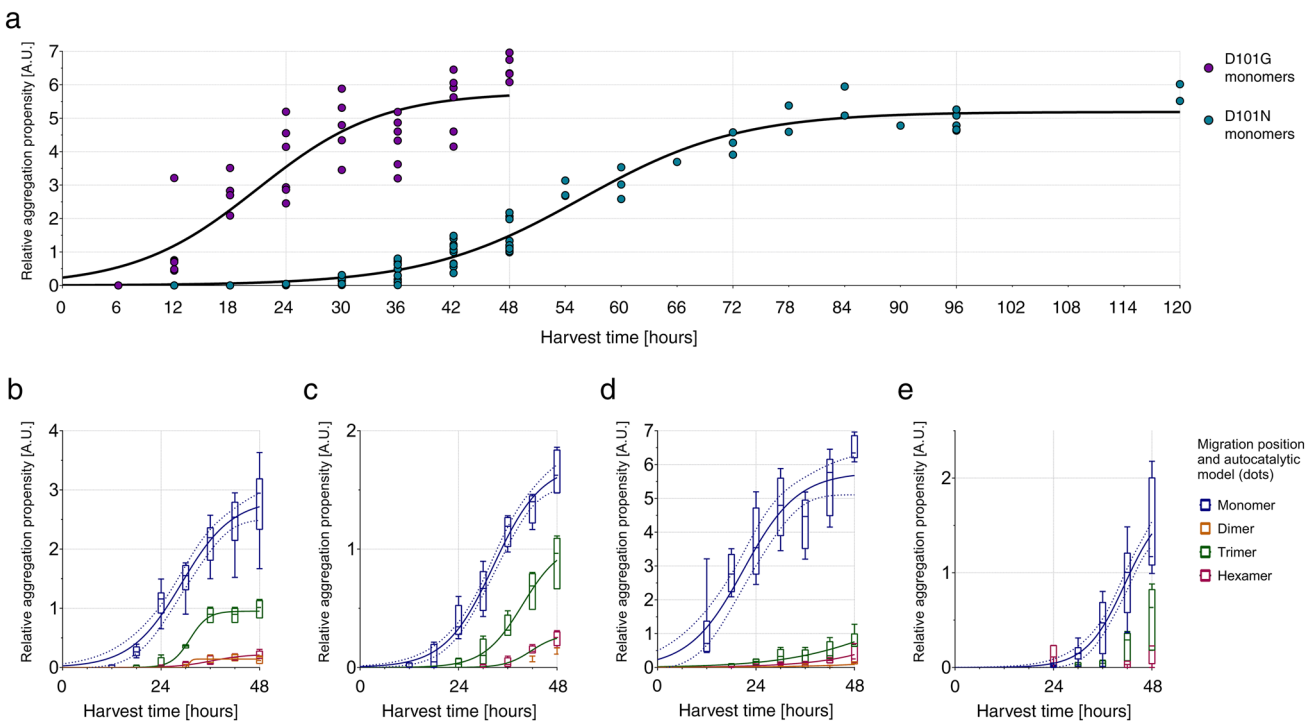

Fig. 3 Quantified time-course results on the relative aggregation propensities of SOD1 variants **b** G85R, **c** G37R, **a**, **d** D101G, and **a**, **e** D101N. **a** Dot plots of D101G and D101N monomers over extended time course of up to 5 days, with a trend line fit according to the autocatalytic function (solid lines); **b-e** Box-and-whiskers plots (minimum, 25th percentile, median, 75th percentile, and maximum) with a trend line fit according to the autocatalytic function (solid lines) and their 95% confidence intervals (dashed lines) of **b** G85R, **c** G37R, **d** D101G, **e** D101N; excluding outliers $Q = 1.0\%$: **b** 0, **c** 3, **d** 2, **e** 0 ($n \geq 4$)

The enzymatic activity of these subsets as detected by NBT/R is given in Fig. 5d. The predicted migration of specific SOD1 subsets as determined by their calculated zeta potential is given in Fig. 5e, which is key to delineating the native electrophoretic graphs of Fig. 5a–d.

The native PAGE immunoblots of Fig. 5a–c were identically and concurrently prepared, except for the βME/SDS in-gel reduction of Fig. 5b and the differing primary antibody application of Fig. 5c. The hrcN-PAGE of Fig. 5d was also identically and concurrently prepared to Fig. 5a–c, except that it was treated with an in-gel NBT/R assay. The NBT/R method was found valid when compared to the results of nearly identical pulse radiolysis experiments. The applied 100cV enables a critical analysis of the SOD1 subsets based on the principle that the subset species have variable migration patterns in PAGE. Migration patterns were delineated by calculating the zeta potential of the expected species at the assay pH, which also varied according to the mutant variant, multimer order, and intra-disulfide bonds; the electrophoretic key derived from this analysis is given in Fig. 5e.

Effect of superoxide radical on a cell culture panel and G85R in HEK293FT

A cell culture panel comprised of N2a, SH-SY5Y, NIH3T3, and HEK293FT was experimentally exposed to high concentrations of superoxide via the cytosolic redox cycler paraquat, as given in Fig. 6. Micrographs of the cell cultures exposed to paraquat are given in Fig. 6a, F/T extracts of endogenous SOD1 in UT culture exposed to paraquat are given in Fig. 6b, and detergent ultracentrifugation extracts of HEK293FT cells that expressed WT and G85R exposed to paraquat are given in Fig. 6c.

Superoxide exposure via paraquat caused extensive vacuolation and cell death as given in the micrographs of Fig. 6a, which were symptomatic of a high cytoplasmic concentration of superoxide. Figure 6b shows that paraquat increased endogenous SOD1 degradation and the formation of trimers and apparent hexamers predominantly in cells from mice (N2a and NIH-3T3) but not necessarily humans (SH-SY5Y and HEK293FT). In the experiments represented by Fig. 6c,

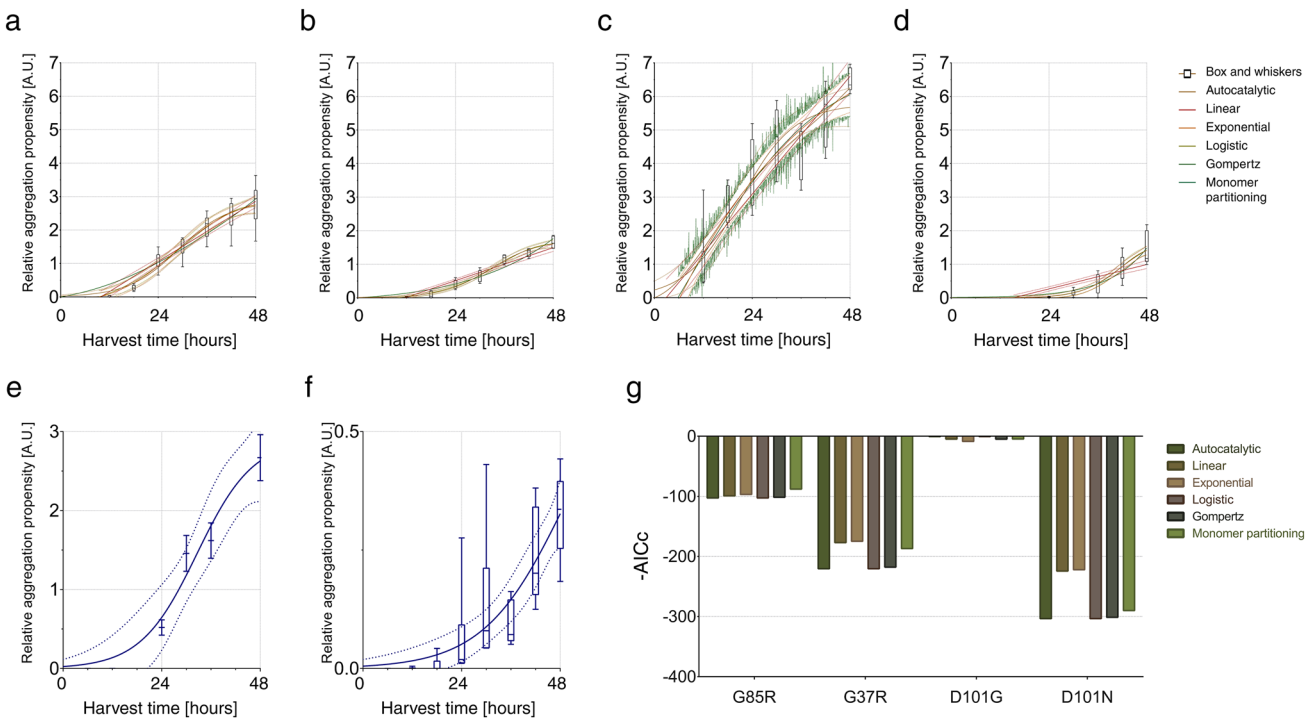

Fig. 4 Statistical analyses of the logistic function of best fit for the relative aggregation propensities of G85R, G37R, D101G, D101N, and G93A and H46R/H48Q at the monomeric position. Box-and-whiskers plots represent ≥ 4 distinct repetitions (minimum, 25th percentile, median, 75th percentile, and maximum). The sigmoid functions (autocatalytic, linear, exponential, logistic, gompertz, and monomer partitioning) are accorded by key. **a-d** Graphical evaluation of the statistical analyses of the relative aggregation propensities for ALS1 variants **a** D101G, **b** D101N, **c** G85R, and **d** G37R, at the monomeric position. **e–f** Relative aggregation propensities at the monomeric position of **e** ALS1 variant G93A and **f** the experimental compound copper ablation variant H46R/H48Q. Data were collected from HEK293FT utilizing the detergent ultracentrifugation method. **e** Mean with SD represent 2 or 3 distinct experiments, and (**f**) Box-and-whiskers plots represent ≥ 4 distinct repetitions (minimum, 25th percentile, median, 75th percentile, and maximum). **g** A functional derivative of AIC (− AICc) was used in this study. The goodness of fit of the sigmoidal functions were programmatically evaluated by a modified variant of the AIC criterion

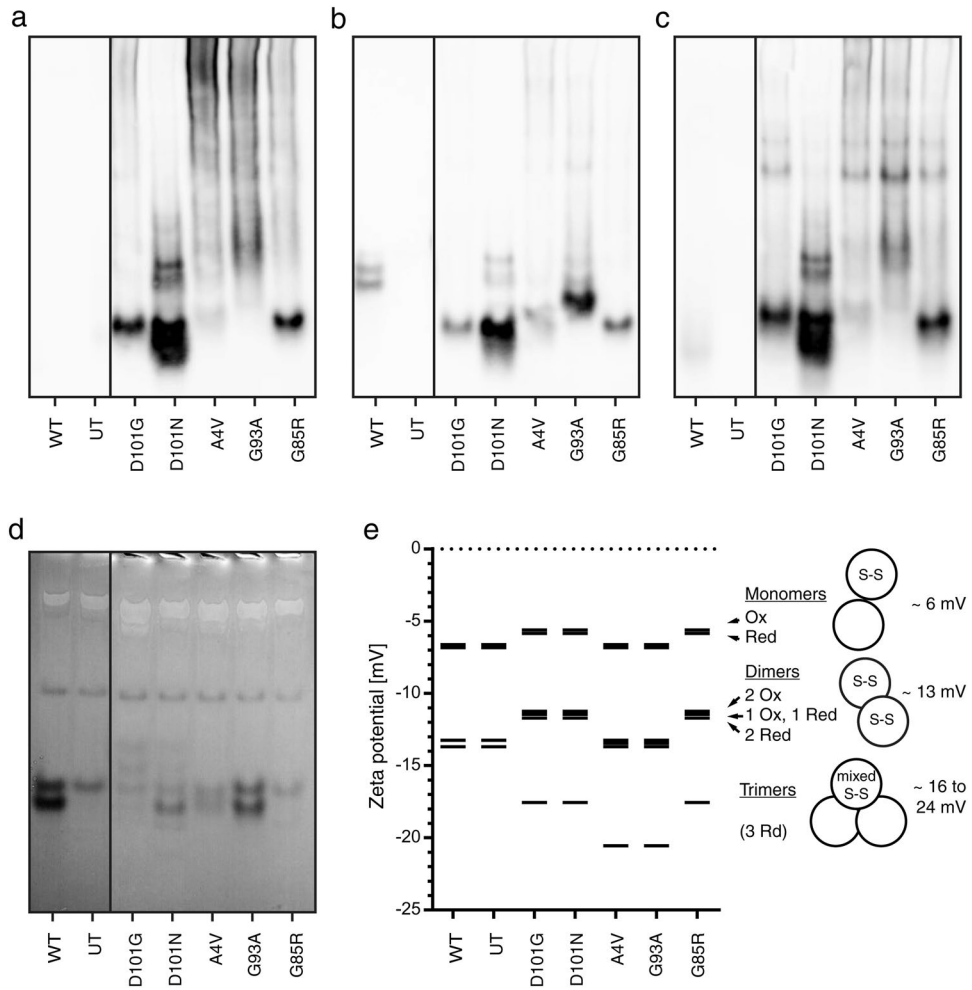

Fig. 5 Molecular properties of ALS1 variants as determined by high-resolution PAGE methods used to delineate the polymer and intra-disulfide oxidation states of the soluble subsets, at a harvest time of 48 h in HEK293FT ($n=2$). 7.5 µg soluble S1 fractions were electrophoresed at pH 7.4 for 8 h at 100cV on a 4–20% PAGE gel. **a** N-PAGE immunoblot with antibody 124–136. **b** N-PAGE immunoblot with antibody 124–136, processed with βME/SDS in-gel reduction. **c** N-PAGE immunoblot with antibody 24–36. **d** NBT/R enzymatic activity assay. **e** Predicted migration of oxidized (Ox) and reduced (Red) subsets of various SOD1 monomers, dimers, and trimers, according to their zeta potentials at pH 7.4

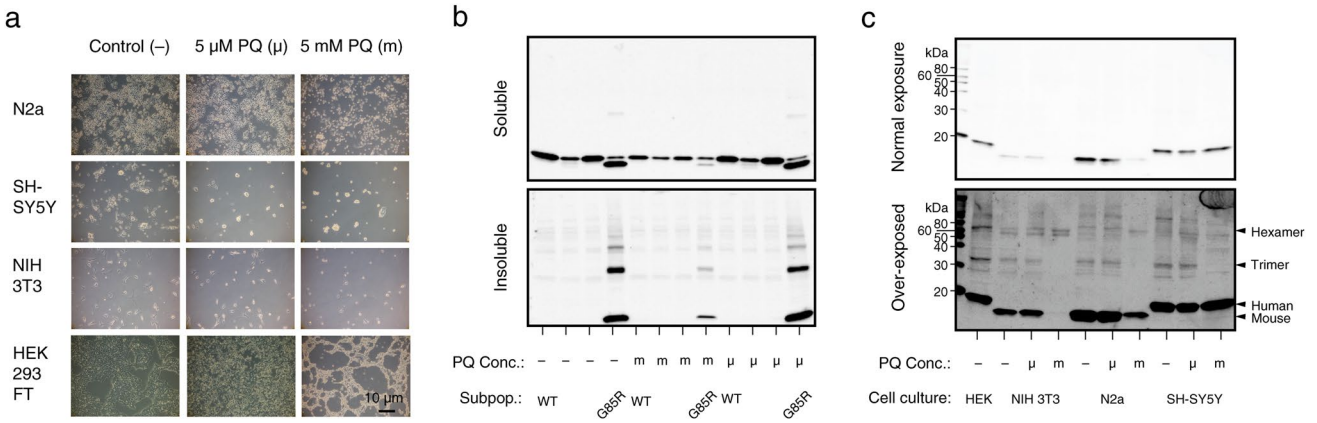

Fig. 6 Superoxide exposures via paraquat, showing that high concentrations of superoxide modulate non-native SOD1 formations across four cultured neuronal cell lines. High-concentration superoxide substrate exposure via 18 h treatment with paraquat on **a** four immortal cell lines with analysis for **b** endogenous SOD1 and **c** G85R expressed in HEK293FT. **a** Representative micrographs of controlled endogenous N2a, SH-SY5Y, NIH-3T3, and HEK-293FT cells (–) as exposed to 5 µM (µ) and 5 mM (m) paraquat (PQ); a 10 µm bar is drawn to scale ($n=2$). **b** Representative western immunoblots of 10 µg endogenous cells that were F/T extracted with 5% βME, with paraquat concentrations indicated, at both normal exposure and over-exposed ($n=3$). **c** Soluble and insoluble standard detergent ultracentrifugation extracts of HEK293FT cells expressing WT and G85R, at variable paraquat concentrations as indicated ($n=2$)

G85R was found to have an untreated relative aggregation propensity of 1.23. 5 μM paraquat exposure to G85R caused a modest increase in the relative aggregation propensity to 1.31, and 5 mM paraquat exposure to G85R caused a drastic increase in the relative aggregation propensity to 4.33.

Discussion

SOD1 is involved in at least two verifiably healthy reactions: its own maturation and the enzymatic dissipation of superoxide. After SOD1 is supplied and activated with the correct component states, its primary molecular function is to prevent the volatile radical exchange reactions of relatively toxic superoxide by expediting its oxidation to innocuous dioxygen. Two determining molecular properties of SOD1 function or dysfunction are the number of subunits in the formation and the intra-disulfide oxidation state of the subunits. Monomeric, intra-disulfide-reduced subsets are particularly vulnerable to nucleation. This immaturity yet senility theory is in the process of superseding misfolding theory because it explains and predicts aggregation mechanisms with a greater comprehension, and its hypotheses are more easily falsifiable. Immature SOD1 that has not yet undergone post-translational processing does not have an oxidized intra-disulfide bond or bound metals and is unable to process superoxide radical. Radicals are attracted to SOD1 by mechanisms of substrate steering and guidance. "Hot spots" accumulate focal charge, which could feasibly nucleate a polymerization reaction not unlike radical polymerizations pervasive elsewhere in bioorganic chemistry. In this work, a panel of four untransfected human and murine immortalized cell culture lines were exposed to high concentrations of superoxide via paraquat. HEK293FT expressing G85R that were then exposed to paraquat under otherwise standard laboratory conditions had a relative aggregation propensity of 4.33, which is significantly higher than without paraquat exposure. My results on paraquat exposures indicate that SOD1 is faster to nucleate in the presence of high concentrations of superoxide radical substrate, with G85R exposed to high-concentration superoxide radical even having the highest aggregation propensity yet recorded out of dozens of different ALS1 variants surveyed under similar conditions.

The SOD1 subsets observed over the time course of maturation have differing multimerization, metallation, and intra-disulfide oxidation states. In this work, I identified correlations between these component subsets and their activity and aggregation. The intra-disulfide-reduced monomer had low activity and high aggregation propensity, whereas the intra-disulfide-oxidized dimer had high activity and low aggregation propensity. An oxidized intra-disulfide bond was apparently necessary for enzymatic activity. Though most ALS1 variant expression sets retain global activity, the intra-disulfide-reduced subsets most implicated in causing ALS1 do not retain their specific activity. A loss of mature subsets implies a loss of dismutase function among these subsets.

Clinical and biochemical forays have shown that every investigated SOD1 implicated in ALS1 studied thus far forms distinct but relatively variable aggregates—observed biochemically and histologically—whereas wild-type and other innocuous SOD1 remain persistently soluble. Therefore, a unifying pathogenicity theory is that proteinaceous SOD1 aggregates are either concomitant with or antecede its toxic effect. The differing variants have heterogeneous aggregation kinetics over the hours and days surveyed post-expression in HEK293FT. SOD1 variant aggregation propensities are extremely heterogeneous. The aggregation metrics are reproducibly dependent on and vary with the identity of the variant. For example, D101N had an irregularly long lag phase, which enabled a closer examination of its temporal nucleation within the aggregation reaction, as given in Fig. 2a.

SOD1 polymerization including aggregation proceed by at least two phases comprised of nucleation and growth. The four logistic phases of the SOD1 aggregation reaction identified herein are lag, nucleation, growth, and plateau. The lag phase is comprised of low multimer subsets including monomers and dimers. Excluding the lag phase (present in both ordinary and pathological pools), there are three punctuated phase controllers: the second-order nucleation of trimers and hexamers, the zero-order growth of senile aggregates, and the zero-order plateau that includes the first fragments. The post-nucleation kinetic results obtained here corroborate the near-linear or pseudo-zeroth-order results seen in test tube experiments nucleated by physicochemical agitation. The nucleation phase proceeds by the aberrant formation of trimers, hexamers, and other apparent 3n species. Lagging subsets are most susceptible to a concerted or punctuated nucleation to low molecular weight multimers and eventual aggregates, as shown by the growth and nucleation data. The fragment observations during the zeroth-order plateau comprise a relatively novel pathogenic hypothesis for SOD1 notwithstanding fragment pathogenicity theories in other hereditary neurodegenerative disease.

The greatest concern of familial ALS research must be finding an effective treatment, but the mechanism by which SOD1 rarely causes ALS1 is uncertain and not yet successfully druggable. This study prefaces an investigation to develop rational drug design hypotheses by new target-validators, for instance, the characterized multimer subsets and proteinaceous radical polymerizations. These findings clarify but do not yet advance the state of the applied science.

Acknowledgements The author thanks David Borchelt for advice and resources.

Author contributions The author designed, performed, and analyzed the experiments and prepared the manuscript.

Compliance with ethical standards

Conflict of interest The author does not have a conflict of interest to declare.

References

1. Pardo CA, Xu Z, Borchelt DR, Price DL, Sisodia SS, Cleveland DW (1995) Superoxide dismutase is an abundant component in cell bodies, dendrites, and axons of motor neurons and in a subset of other neurons. Proc Natl Acad Sci USA 92:954–958
2. Dupeyrat F, Vidaud C, Lorphelin A, Berthomieu C (2004) Long distance charge redistribution upon Cu, Zn-superoxide dismutase reduction: significance for dismutase function. J Biol Chem 279:48091–48101
3. Rotilio G, Bray RC, Fielden EM (1972) A pulse radiolysis study of superoxide dismutase. Biochim Biophys Acta 268:605–609
4. Forman HJ, Fridovich I (1973) Superoxide dismutase: a comparison of rate constants. Arch Biochem Biophys 158:396–400
5. Reddi AR, Culotta VC (2013) SOD1 integrates signals from oxygen and glucose to repress respiration. Cell 152:224–235
6. Liochev SI, Fridovich I (2000) Copper- and zinc-containing superoxide dismutase can act as a superoxide reductase and a superoxide oxidase. J Biol Chem 275:38482–38485
7. Workman AS (2017) Real-time TD-DFT study on the dioxygen/superoxide radical charge transfer reaction. Comput Theor Chem 1117:207–214
8. Nedd S, Redler RL, Proctor EA, Dokholyan NV, Alexandrova AN (2014) Cu, Zn-superoxide dismutase without Zn is folded but catalytically inactive. J Mol Biol 426:4112–4124
9. Banci L, Bertini I, Cantini F, Kozyreva T, Massagni C, Palumaa P, Rubino JT, Zovo K (2012) Human superoxide dismutase 1 (hSOD1) maturation through interaction with human copper chaperone for SOD1 (hCCS). Proc Natl Acad Sci USA 109:13555–13560
10. Girotto S, Cendron L, Bisaglia M, Tessari I, Mammi S, Zanotti G, Bubacco L (2014) DJ-1 is a copper chaperone acting on SOD1 activation. J Biol Chem 289:10887–10899
11. Culotta VC, Klomp LW, Strain J, Casareno RLB, Krems B, Gitlin JD (1997) The copper chaperone for superoxide dismutase. J Biol Chem 272:23469–23472
12. Banci L, Cantini F, Kozyreva T, Rubino JT (2013) Mechanistic aspects of hSOD1 maturation from the solution structure of CuI-Loaded hCCS domain 1 and analysis of disulfide-free hSOD1 mutants. ChemBioChem 14:1839–1844
13. Leitch JM, Jensen LT, Bouldin SD, Outten CE, Hart PJ, Culotta VC (2009) Activation of Cu, Zn-superoxide dismutase in the absence of oxygen and the copper chaperone CCS. J Biol Chem 284:21863–21871
14. Brown NM, Torres AS, Doan PE, O'Halloran TV (2004) Oxygen and the copper chaperone CCS regulate posttranslational activation of Cu, Zn superoxide dismutase. Proc Natl Acad Sci USA 101:5518–5523
15. Seetharaman SV, Prudencio M, Karch C, Holloway SP, Borchelt DR, Hart PJ (2009) Immature copper–zinc superoxide dismutase and familial amyotrophic lateral sclerosis. Exp Biol Med 234:1140–1154
16. Hörnberg A, Logan DT, Marklund SL, Oliveberg M (2007) The coupling between disulphide status, metallation and dimer interface strength in Cu/Zn superoxide dismutase. J Mol Biol 365:333–342
17. Furukawa Y, Torres AS, O'Halloran TV (2004) Oxygen-induced maturation of SOD1: a key role for disulfide formation by the copper chaperone CCS. EMBO J 23:2872–2881
18. Saccon RA, Bunton-Stasyshyn RK, Fisher EM, Fratta P (2013) Is SOD1 loss of function involved in amyotrophic lateral sclerosis? Brain 136:2342–2358
19. Bunton-Stasyshyn RK, Saccon RA, Fratta P, Fisher EM (2015) SOD1 function and its implications for amyotrophic lateral sclerosis pathology: new and renascent themes. Neuroscientist 21:519–529
20. Grad LI, Rouleau GA, Ravits J, Cashman NR (2017) Clinical spectrum of amyotrophic lateral sclerosis (ALS). Cold Spring Harb Perspect Med
21. Black HA, Leighton DJ, Cleary EM, Rose E, Stephenson L, Colville S, Ross D, Warner J, Porteous M, Gorrie GH, Swingler R, Goldstein D, Harms MB, Connick P, Pal S, Aitman TJ, Chandran S (2016) Genetic epidemiology of motor neuron disease-associated variants in the Scottish population. Neurobiol Aging 51:178
22. Finsterer J, Burgunder J (2014) Recent progress in the genetics of motor neuron disease. Eur J Med Genet 57:103–112
23. Abel O, Powell JF, Andersen PM, Al-Chalabi A (2012) ALSoD: a user-friendly online bioinformatics tool for amyotrophic lateral sclerosis genetics. Hum Mutat 33:1345–1351
24. Rosen DR, Siddique T, Patterson D, Figlewicz DA, Sapp P, Hentati A, Donaldson D, Goto J, O'Regan JP, Deng H, Rahmani Z, Krizus A, McKenna-Yasek D, Cayabyab A, Gaston SM, Berger R, Tanzi RE, Halperin JJ, Herzfeldt B, Van dB, Hung W, Bird T, Deng G, Mulder DW, Smyth C, Laing NG, Soriano E, Pericak-Vance M, Haines J, Rouleau GA, Gusella JS, Horvitz HR, Brown RH, (1993) Mutations in Cu/Zn superoxide dismutase gene are associated with familial amyotrophic lateral sclerosis. Nature 362(6415):59–62
25. Wang J, Xu G, Slunt HH, Gonzales V, Coonfield M, Fromholt D, Copeland NG, Jenkins NA, Borchelt DR (2005) Coincident thresholds of mutant protein for paralytic disease and protein aggregation caused by restrictively expressed superoxide dismutase cDNA. Neurobiol Dis 20:943–952
26. Andersen PM (2006) Amyotrophic lateral sclerosis associated with mutations in the CuZn superoxide dismutase gene. Curr Neurol Neurosci Rep 6:37–46
27. Borchelt DR, Lee MK, Slunt HS, Guarnieri M, Xu ZS, Wong PC, Brown RH Jr, Price DL, Sisodia SS, Cleveland DW (1994) Superoxide dismutase 1 with mutations linked to familial amyotrophic lateral sclerosis possesses significant activity. Proc Natl Acad Sci USA 91:8292–8296
28. Prudencio M, Hart PJ, Borchelt DR, Andersen PM (2009) Variation in aggregation propensities among ALS-associated variants of SOD1: correlation to human disease. Hum Mol Genet 18:3217–3226
29. Ayers J, Lelie H, Workman A, Prudencio M, Brown H, Fromholt S, Valentine J, Whitelegge J, Borchelt D (2013) Distinctive features of the D101N and D101G variants of superoxide dismutase 1; two mutations that produce rapidly progressing motor neuron disease. J Neurochem 128:305–314
30. Bystrom R, Andersen PM, Grobner G, Oliveberg M (2010) SOD1 mutations targeting surface hydrogen bonds promote amyotrophic lateral sclerosis without reducing apo-state stability. J Biol Chem 285:19544–19552

31. Bruijn L, Becher M, Lee M, Anderson K, Jenkins N, Copeland N, Sisodia S, Rothstein J, Borchelt D, Price D (1997) ALS-linked SOD1 mutant G85R mediates damage to astrocytes and promotes rapidly progressive disease with SOD1-containing inclusions. Neuron 18:327–338
32. Wang J, Caruano-Yzermans A, Rodriguez A, Scheurmann JP, Slunt HH, Cao X, Gitlin J, Hart PJ, Borchelt DR (2007) Disease-associated mutations at copper ligand histidine residues of superoxide dismutase 1 diminish the binding of copper and compromise dimer stability. J Biol Chem 282:345–352
33. Winkler DD, Schuermann JP, Cao X, Holloway SP, Borchelt DR, Carroll MC, Proescher JB, Culotta VC, Hart PJ (2009) Structural and biophysical properties of the pathogenic SOD1 variant H46R/H48Q. Biochemistry 48:3436–3447
34. Elam JS, Taylor AB, Strange R, Antonyuk S, Doucette PA, Rodriguez JA, Hasnain SS, Hayward LJ, Valentine JS, Yeates TO (2003) Amyloid-like filaments and water-filled nanotubes formed by SOD1 mutant proteins linked to familial ALS. Nat Struct Mol Biol 10:461–467
35. Ray SS, Nowak RJ, Strokovich K, Brown RH, Walz T, Lansbury PT (2004) An intersubunit disulfide bond prevents in vitro aggregation of a superoxide dismutase-1 mutant linked to familial amytrophic lateral sclerosis. Biochemistry 43:4899–4905
36. Rakhit R, Crow JP, Lepock JR, Kondejewski LH, Cashman NR, Chakrabartty A (2004) Monomeric Cu, Zn-superoxide dismutase is a common misfolding intermediate in the oxidation models of sporadic and familial amyotrophic lateral sclerosis. J Biol Chem 279:15499–15504
37. Svensson AE, Bilsel O, Kayatekin C, Adefusika JA, Zitzewitz JA, Matthews CR (2010) Metal-free ALS variants of dimeric human Cu, Zn-superoxide dismutase have enhanced populations of monomeric species. PLoS ONE 5:e10064
38. Banci L, Bertini I, Durazo A, Girotto S, Gralla EB, Martinelli M, Valentine JS, Vieru M, Whitelegge JP (2007) Metal-free superoxide dismutase forms soluble oligomers under physiological conditions: a possible general mechanism for familial ALS. Proc Natl Acad Sci USA 104:11263–11267
39. Kayatekin C, Zitzewitz JA, Matthews CR (2010) Disulfide-reduced ALS variants of Cu, Zn superoxide dismutase exhibit increased populations of unfolded species. J Mol Biol 398:320–331
40. Abdolvahabi A, Shi Y, Chuprin A, Rasouli S, Shaw BF (2016) Stochastic formation of fibrillar and amorphous superoxide dismutase oligomers linked to amyotrophic lateral sclerosis. ACS Chem Neurosci 7:799–810
41. Karch CM, Prudencio M, Winkler DD, Hart PJ, Borchelt DR (2009) Role of mutant SOD1 disulfide oxidation and aggregation in the pathogenesis of familial ALS. Proc Natl Acad Sci USA 106:7774–7779
42. Shaw BF, Lelie HL, Durazo A, Nersissian AM, Xu G, Chan PK, Gralla EB, Tiwari A, Hayward LJ, Borchelt DR, Valentine JS, Whitelegge JP (2008) Detergent-insoluble aggregates associated with amyotrophic lateral sclerosis in transgenic mice contain primarily full-length, unmodified superoxide dismutase-1. J Biol Chem 283:8340–8350
43. Wang J, Xu G, Borchelt DR (2002) High molecular weight complexes of mutant superoxide dismutase 1: age-dependent and tissue-specific accumulation. Neurobiol Dis 9:139–148
44. Wang J, Farr GW, Zeiss CJ, Rodriguez-Gil DJ, Wilson JH, Furtak K, Rutkowski DT, Kaufman RJ, Ruse CI, Yates JR, Perrin S, Feany MB, Horwich AL (2009) Progressive aggregation despite chaperone associations of a mutant SOD1-YFP in transgenic mice that develop ALS. Proc Natl Acad Sci USA 106(5):1392–1397
45. Wang J, Xu G, Gonzales V, Coonfield M, Fromholt D, Copeland NG, Jenkins NA, Borchelt DR (2002) Fibrillar inclusions and motor neuron degeneration in transgenic mice expressing superoxide dismutase 1 with a disrupted copper-binding site. Neurobiol Dis 10:128–138
46. Ratovitski T, Corson LB, Strain J, Wong P, Cleveland DW, Culotta VC, Borchelt DR (1999) Variation in the biochemical/biophysical properties of mutant superoxide dismutase 1 enzymes and the rate of disease progression in familial amyotrophic lateral sclerosis kindreds. Hum Mol Genet 8:1451–1460
47. Synofzik M, Ronchi D, Keskin I, Basak AN, Wilhelm C, Gobbi C, Birve A, Biskup S, Zecca C, Fernandez-Santiago R, Kaugesaar T, Schols L, Marklund SL, Andersen PM (2012) Mutant superoxide dismutase-1 indistinguishable from wild-type causes ALS. Hum Mol Genet 21:3568–3574
48. Wang Q, Johnson JL, Agar NY, Agar JN (2008) Protein aggregation and protein instability govern familial amyotrophic lateral sclerosis patient survival. PLoS Biol 6:e170
49. Parge HE, Hallewell RA, Tainer JA (1992) Atomic structures of wild-type and thermostable mutant recombinant human Cu, Zn superoxide dismutase. Proc Natl Acad Sci USA 89:6109–6113
50. Getzoff ED, Cabelli DE, Fisher CL, Parge HE, Viezzoli MS, Banci L, Hallewell RA (1992) Faster superoxide dismutase mutants designed by enhancing electrostatic guidance. Nature 358:347–351
51. Cleveland DW, Liu J (2000) Oxidation versus aggregation-how do SOD1 mutants cause ALS? Nat Med 6:1320–1321
52. Salo DC, Pacifici RE, Lin SW, Giulivi C, Davies KJ (1990) Superoxide dismutase undergoes proteolysis and fragmentation following oxidative modification and inactivation. J Biol Chem 265:11919–11927
53. Cocheme HM, Murphy MP (2008) Complex I is the major site of mitochondrial superoxide production by paraquat. J Biol Chem 283:1786–1798
54. Turner BJ, Lopes EC, Cheema SS (2004) Inducible superoxide dismutase 1 aggregation in transgenic amyotrophic lateral sclerosis mouse fibroblasts. J Cell Biochem 91:1074–1084
55. Khare SD, Caplow M, Dokholyan NV (2004) The rate and equilibrium constants for a multistep reaction sequence for the aggregation of superoxide dismutase in amyotrophic lateral sclerosis. Proc Natl Acad Sci USA 101:15094–15099
56. Hong S, Lee S, Choi I, Yang YI, Kang T, Yi J (2013) Real-time analysis and direct observations of different superoxide dismutase (SOD1) molecules bindings to aggregates in temporal evolution step. Colloids Surf B 101:266–271
57. McAlary L, Aquilina JA, Yerbury JJ (2016) Susceptibility of mutant SOD1 to form a destabilized monomer predicts cellular aggregation and toxicity but not in vitro aggregation propensity. Front Neurosci 10:499
58. Lang L, Zetterstrom P, Brannstrom T, Marklund SL, Danielsson J, Oliveberg M (2015) SOD1 aggregation in ALS mice shows simplistic test tube behavior. Proc Natl Acad Sci USA 112:9878–9883
59. Karch CM, Borchelt DR (2008) A limited role for disulfide cross-linking in the aggregation of mutant SOD1 linked to familial amyotrophic lateral sclerosis. J Biol Chem 283:13528–13537
60. Wang J, Slunt H, Gonzales V, Fromholt D, Coonfield M, Copeland NG, Jenkins NA, Borchelt DR (2003) Copper-binding-site-null SOD1 causes ALS in transgenic mice: aggregates of non-native SOD1 delineate a common feature. Hum Mol Genet 12:2753–2764
61. Mizushima S, Nagata S (1990) pEF-BOS, a powerful mammalian expression vector. Nucleic Acids Res 18:5322
62. Prudencio M, Lelie H, Brown HH, Whitelegge JP, Valentine JS, Borchelt DR (2012) A novel variant of human superoxide dismutase 1 harboring amyotrophic lateral sclerosis-associated

and experimental mutations in metal-binding residues and free cysteines lacks toxicity in vivo. J Neurochem 121:475–485
63. Henderson LJ (1908) Concerning the relationship between the strength of acids and their capacity to preserve neutrality. Am J Physiol 21:173–179
64. Hasselbalch KA (1916) Die berechnung der wasserstoffzahl des blutes aus der freien und gebundenen Kohlensäure desselben, und die sauerstoffbindung des blutes als funktion der wasserstoffzahl. Springer, Berlin
65. Chauhan OP, Singh S (1992) Order of reaction for sigmoidal curves. Biochem Educ 20:230–230
66. Akaike H (1978) On the likelihood of a time series model. Stat 27(3–4):217–235